Journal of Physics: Condensed Matter

PAPER

Transformation from an easy-plane to an easy-axis antiferromagnetic structure in the mixed rare-earth ferroborates $Pr_xY_{1-x}Fe_3(BO_3)_4$: magnetic properties and crystal field calculations

To cite this article: A I Pankrats *et al* 2016 *J. Phys.: Condens. Matter* **28** 396001

IOP Publishing Journal of Physics: Condensed Matter
J. Phys.: Condens. Matter **28** (2016) 396001 (18pp) doi:10.1088/0953-8984/28/39/396001

Transformation from an easy-plane to an easy-axis antiferromagnetic structure in the mixed rare-earth ferroborates $Pr_xY_{1-x}Fe_3(BO_3)_4$: magnetic properties and crystal field calculations

A I Pankrats[1], A A Demidov[2], C Ritter[3], D A Velikanov[1], S V Semenov[1], V I Tugarinov[1], V L Temerov[1] and I A Gudim[1]

[1] Kirensky Institute of Physics, Siberian Branch of RAS, 660036 Krasnoyarsk, Russia
[2] Bryansk State Technical University, 241035 Bryansk, Russia
[3] Institut Laue-Langevin, BP 156, F-38042 Grenoble, France

E-mail: demandr@yandex.ru

Received 2 April 2016, revised 21 June 2016
Accepted for publication 22 June 2016
Published 1 August 2016

Abstract

The magnetic structure of the mixed rare-earth system $Pr_xY_{1-x}Fe_3(BO_3)_4$ ($x = 0.75$, 0.67, 0.55, 0.45, 0.25) was studied via magnetic and resonance measurements. These data evidence the successive spin reorientation from the easy-axis antiferromagnetic structure formed in $PrFe_3(BO_3)_4$ to the easy-plane one of $YFe_3(BO_3)_4$ associated with the weakening of the magnetic anisotropy of the Pr subsystem due to its diamagnetic dilution by nonmagnetic Y. This reorientation occurs through the formation of an inclined magnetic structure, as was confirmed by our previous neutron research in the range of $x = 0.67 \div 0.45$. In the compounds with $x = 0.75$ and 0.67 whose magnetic structure is close to the easy-axis one, a two-step spin reorientation takes place in the magnetic field $\mathbf{H} \| \mathbf{c}$. Such a peculiarity is explained by the formation of an interjacent inclined magnetic structure with magnetic moments of Fe ions located closer to the basal plane than in the initial state, with these intermediate states remaining stable in some ranges of the magnetic field.

An approach based on a crystal field model for the Pr^{3+} ion and the molecular-field approximation is used to describe the magnetic characteristics of the system $Pr_xY_{1-x}Fe_3(BO_3)_4$. With the parameters of the *d–d* and *f–d* exchange interactions, of the magnetic anisotropy of the iron subsystem and of the crystal field parameters of praseodymium thus determined, it is possible to achieve a good agreement between the experimental and calculated temperature and field dependences of the magnetization curves (up to 90 kOe) and magnetic susceptibilities (2–300 K).

Keywords: magnetic phase transitions, rare-earth ferroborates $RFe_3(BO_3)_4$, antiferromagnetic resonance

(Some figures may appear in colour only in the online journal)

1. Introduction

Rare-earth ferroborates $RFe_3(BO_3)_4$ (R = Y, La–Lu) are of great interest for the physics of magnetic phenomena as compounds with two types of magnetic ions (3*d* and 4*f*) which exhibit a variety of magnetic phase transitions (see e.g. [1–5]). It has been established that the ferroborates $RFe_3(BO_3)_4$ belong to the class of multiferroics in which the elastic, magnetic and

electrical order parameters coexist [1, 3, 4]. Crystallizing in the non-centrosymmetric trigonal space group $R32$ a structural transition to $P3_121$ can take place on cooling at a temperature depending linearly on the rare-earth ionic radius [6, 7]. Due to the polarizing effect of the iron subsystem on the rare-earth one, the magnetic anisotropy of $RFe_3(BO_3)_4$ compounds is determined by the contributions of both subsystems. It is known [8] that the magnetic anisotropy of the Fe subsystem is easy plane (EP), with the magnetic moments of the Fe^{3+} ions lying in the basal plane. Depending on the magnitude and the sign of the anisotropic contribution of the rare-earth subsystem, the resulting easy-axis (EA) or EP magnetic structures can be established in the crystal[4] [8–10]. As the detailed neutron scattering and magnetic x-ray scattering results show, however, these structures can also be slightly non-collinear (R = Ho [8] and Er[4] [10]) or long-period incommensurate (R = Nd [11] and Gd above 10 K [12]).

Interest in the study of the mixed rare-earth ferroborates $R^{(1)}_xR^{(2)}_{1-x}Fe_3(BO_3)_4$, $RFe_{3-x}Ga_x(BO_3)_4$ and $R_xY_{1-x}Fe_3(BO_3)_4$ arises from the ability to control the relative contributions with which the R and Fe subsystems influence the magnetic and other properties of the crystal. The magnetic anisotropy of the mixed compounds with $R = Nd_xDy_{1-x}$ has been shown to also be determined by the competition between the EP contributions from the Nd^{3+} and Fe^{3+} ions on the one hand and the EA contribution from the Dy^{3+} ions on the other. As a result, spontaneous reorientation transitions between EP and EA states also occur in these complex crystals with the temperature T_{SR} depending on x [13].

The relation between the competing contributions can also be changed by a diamagnetic dilution of one of the subsystems reducing the contribution of this subsystem to the crystal anisotropy. Thus, in a crystal with R = Gd, the diamagnetic dilution of the iron subsystem with Ga^{3+} ions reduces the anisotropic contribution of the Fe^{3+} subsystem. As a result, the contribution of the gadolinium subsystem appears to be prevalent and, in the absence of a magnetic field, the crystal $GdFe_{3-x}Ga_x(BO_3)_4$ remains EA antiferromagnet in the entire range of magnetic ordering [14].

If an R ion with EA anisotropy is used in diluted ferroborates $R_xY_{1-x}Fe_3(BO_3)_4$, the competition between the contributions of the iron (stabilizing EP state) and R subsystems to the total magnetic anisotropy can cause spontaneous or induced spin-reorientation transitions.

The Fe subsystem in pure $YFe_3(BO_3)_4$ is ferromagnetically ordered in the basal ab-plane with the magnetic moments lying in the plane and adjacent planes in the direction of the rhombohedral c axis being antiferromagnetically aligned [8, 15, 16]. In $PrFe_3(BO_3)_4$, the contribution of the Pr^{3+} ions to the magnetic anisotropy of the crystal is prevalent and defines an EA antiferromagnetic structure at all temperatures below the Neel temperature $T_N = 32$ K [10, 17]. Thus, as a result of the competition between different contributions to the magnetic anisotropy of $Pr_xY_{1-x}Fe_3(BO_3)_4$, a rearrangement of the magnetic structure between EA and EP states should appear.

High-resolution and temperature-dependent high-intensity powder neutron diffraction studies on $Pr_xY_{1-x}Fe_3(BO_3)_4$ showed that a transition from the EA to the EP structure occurs in this family through the formation of inclined (INC) magnetic structures in the concentration range $x = 0.67 - 0.45$ [18]. This INC state had not been observed before in ferroborates. For all compounds, a non-monotonic change of the inclination angle with temperature was found, but none of the samples studied displayed signs of a spontaneous spin reorientation in the temperature range of magnetic order. A calculation based on a crystal field model for the Pr^{3+} ions and a molecular field approximation allowed the inclination of the magnetic moments of Fe ions from the basal plane and their temperature dependences in the INC state to be described.

To further study the INC phase as a new magnetic state in ferroborates and its transformation with diamagnetic Y dilution, we undertook a wide experimental and theoretical investigation of the magnetic properties of $Pr_xY_{1-x}Fe_3(BO_3)_4$ single crystals with a large set of concentrations $x = 1$, 0.75, 0.67, 0.55, 0.45 and 0.25. The data show the gradual transition of magnetization and susceptibility curves that are typical of the EA structure in $PrFe_3(BO_3)_4$ to those of the EP one in $YFe_3(BO_3)_4$ through the formation of the INC state in crystals with intermediate concentration parameters x. An unusual two-step spin-reorientation transition is found in the compounds with $x = 0.75$ and 0.67 when applying the magnetic field along the c axis. The effect is explained by the formation of an interjacent INC state with an inclination angle that is less than that of the initial state.

Preliminary results of the antiferromagnetic resonance (AFMR) for compounds with $x = 1$, 0.75 and 0.67 that provide evidence of the INC magnetic structure in the compound with $x = 0.75$ are presented.

2. Experiment details

2.1. Sample preparation

Samples were prepared at the Institute of Physics in Krasnoyarsk. Single crystals were grown from fluxes based on trimolibdate bismuth $(100 - n)$ mass% $\{Bi_2Mo_3O_{12} + 3^{11}B_2O_3 + 0.5[xPr_2O_3 + (1 - x)Y_2O_3]\} + n$ mass% $Pr_xY_{1-x}Fe_3(^{11}BO_3)_4$ [19]. For the concentration $n = 20$, the saturation temperature T_s was $T_s \approx 950$ °C and its concentration dependence can be described as $dT_s/dn \approx 6$ °C/mass%. Fluxes with a mass of 100 g were prepared. Crystals were grown on seeds at a starting temperature $T = T_s - 7$ °C, with the temperature reduced by 1 °C d^{-1} over 5 d. Single crystals of about 4–6 mm in size were grown. After completion of the crystallization process the holder with the grown crystals was usually removed quickly from the furnace, leading to a high rate of cooling to room temperature. Only the part of the crystals with $x = 0.67$ was slowly cooled along with the furnace after it had been switched off.

[4] Table 1 of [10] contains some errors. The right-hand side (marked 'Er') of the table (not the left-hand side) corresponds to $PrFe_3(BO_3)_4$, and the values of the lattice parameters given are wrong and correspond to the Ho compound. The atomic coordinates and interatomic distances are correct.

2.2. Magnetization and resonance measurements

Magnetic measurements were performed at the Institute of Physics in Krasnoyarsk, principally using the magnetic and physical property measurement systems MPMS-5 and PPMS-6000 (Quantum Design). The temperature interval was 2–300 K in magnetic fields of up to 50 kOe for MPMS-5 and up to 90 kOe for PPMS-6000. Some samples were also studied using a homemade vibrating sample magnetometer operating in the temperature range of 4.2–300 K and in magnetic fields of up to 70 kOe.

For the preliminary study of AFMR in single crystals at $T = 4.2$ K and in a frequency range of 25 ÷ 110 GHz, a computer-controlled magnetic resonance spectrometer with a pulsed magnetic field was used.

3. Results and discussion

Before discussing the results from the magnetization and resonance experiments we have to recall the most important conclusions from a previous neutron diffraction study [18]. The crystallographic structure of $YFe_3(BO_3)_4$ within the paramagnetic state can be described—as expected from the above-mentioned linear trend for the structural transition temperature—as a function of the R^{3+} ionic radius [6] within the space group $R32$ at 520 K and within the space group $P3_121$ at room temperature and below [8]. In accordance with [6], $PrFe_3(BO_3)_4$ crystallizes in the space group $R32$ at all temperatures down to 1.5 K[4] [10]. The three mixed compounds with $x = 0.45$, 0.55 and 0.67 crystallize at room temperature in the space group $R32$, as expected from the calculated average R^{3+} size. Following [6], the $x = 0.67$ compound should not undergo a transition to $P3_121$ on lowering the temperature, while a transition should appear for the $x = 0.55$ and 0.45 compounds at estimated temperatures of about 65 K and 140 K, respectively. In contrast to this, the crystallographic structure of all three compounds is determined as $R32$ in the whole temperature range, as none of the superlattice peaks typical for the transition from $R32$ to $P3_121$ are detected down to 3 K. Crystallographic details for the series of $Pr_xY_{1-x}Fe_3(BO_3)_4$ compounds can be found in table 1 in [18].

In [18] it was shown that while the magnetic structure of the $x = 0$ compound $YFe_3(BO_3)_4$ consists of a collinear alignment of the Fe moments within the basal *ab*-plane, $Pr_{0.67}Y_{0.33}Fe_3(BO_3)_4$ sees a spin canting of the moments towards the basal plane, resulting in an INC spin structure state with magnetic moment values of $\mu^{Fe} = 4.2(1)\ \mu_B$ and $\mu^{Pr} = 0.8(3)\ \mu_B$ [5].The inclination of the Fe moment from the basal plane at $T = 1.5$ K is equal to $\theta^{Fe} = 67(2)°$.

In contrast to compound 0.67, the basal plane component μ_x^{Fe} in $Pr_{0.55}Y_{0.45}Fe_3(BO_3)_4$ becomes larger than the component in the c direction μ_z^{Fe}, and the inclination of the Fe moment from the basal plane reduces to $\theta^{Fe} = 27(2)°$ at the lowest temperature. At 1.5 K the magnetic moments amount to $\mu^{Fe} = 4.5(1)\ \mu_B$ and $\mu^{Pr} = 0.4(4)\ \mu_B$. As the Pr content is further reduced to $x = 0.45$ it is no longer possible to detect any magnetic moment at low temperatures on the Pr site. Only the Fe sublattice seems to be magnetically long-range ordered with $\mu^{Fe} = 4.2(1)\ \mu_B$. As expected, the magnetic structure approaches even further than the one found for $YFe_3(BO_3)_4$. The component of the Fe moment that points in the direction of the c axis μ_z^{Fe} is further reduced and the inclination angle decreases to about $\theta^{Fe} = 16(4)°$ at 3 K.

High-intensity neutron diffraction data for $Pr_{0.67}Y_{0.33}Fe_3(BO_3)_4$ showed that both the Fe and the Pr magnetizations appear at the same Neel temperature $T_N \approx 31$ K and that their evolution seems to be steady. Only when the individual components of the Fe moment are inspected can a slight change in the temperature evolution of its basal plane component be discerned at about 10 K and explained by the non-monotonic temperature dependence of the inclination angle of the Fe moment from the basal plane. As in other rare-earth ferroborates with a hantite structure, the long antiferromagnetic order appearing in the Fe magnetic subsystem at T_N also induces the respective antiferromagnetic order in the Pr subsystem, leading to the common Neel temperature. The other two compounds with $x = 0.55$ and 0.45 studied by neutrons also showed no signs of a spontaneous spin arrangement up to the Neel temperatures $T_N \approx 30.2$ and 31 K, respectively.

Figure 1 shows the experimental magnetization curves $M_{c,\perp}(H)$ of the crystals $Pr_xY_{1-x}Fe_3(BO_3)_4$ ($x = 0.75$, 0.67, 0.55, 0.45, 0.25) measured at $T = 2$ K for the direction of the magnetic field along the trigonal axis $\mathbf{H}\|\mathbf{c}$ (a) and in the basal plane $\mathbf{H}\perp\mathbf{c}$ (b). The temperature dependences of the initial magnetic susceptibility $\chi_{c,\perp}(T)$ for the corresponding compounds measured in the fields $H_{c,\perp} = 1$ kOe are depicted in figure 2. For comparison, the appropriate field and temperature dependences for the $PrFe_3(BO_3)_4$ and $YFe_3(BO_3)_4$ compounds are also shown in figures 1 and 2. Note that the experimental curves $M_{c,\perp}(H)$ and $\chi_{c,\perp}(T)$ obtained here for pure $PrFe_3(BO_3)_4$ using PPMS-9 in magnetic fields up to 90 kOe generally coincide with those measured in fields up to 50 kOe with a SQUID magnetometer [17].

Analysis of both the temperature and the field dependences shows that the curves are arranged in accordance with the sequential change in the parameter $x = 0.75 \div 0.25$ and are located between the curves for compounds with $x = 1$ and 0. Note that the field dependences of the magnetization measured along the trigonal axis for compounds with $x = 0.75$ and 0.67 (see figure 1(a)) as well as for undiluted crystals with $x = 1$ have a step-like form that is characteristic of a spin-reorientation transition, indicating a resemblance between their magnetic structures. The critical field of the spin-flop (SF) transition in pure $PrFe_3(BO_3)_4$ (≈46 kOe) is much larger than that of the other compounds, and it can be seen clearly from figure 1(a) that in the fields $H > 47$ kOe the curves for all $x = 0.75 \div 0.25$ are arranged sequentially between $M_c(H)$ for $x = 1$ and 0 in accordance with the rule that the higher the Pr-content, the higher the susceptibility. In fields up to the

[5] The magnetic moment value μ^{Pr} here corresponds to the magnetic moment per actual Pr^{3+} ion present.

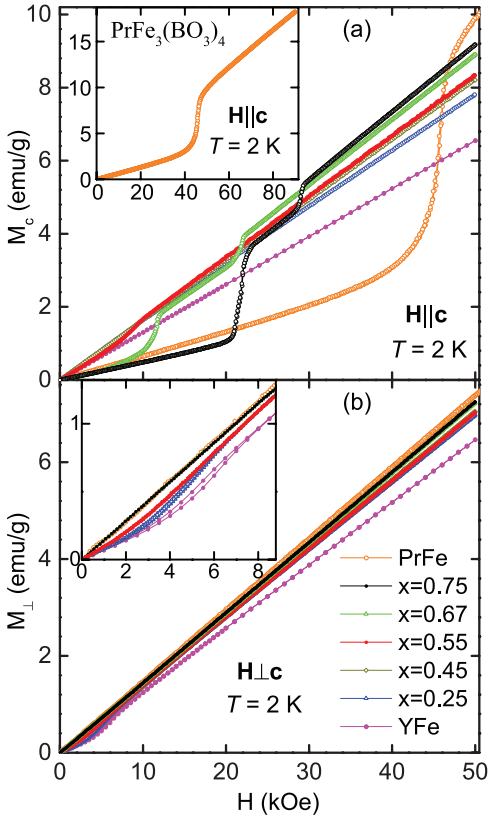

Figure 1. Experimental magnetization curves $M_{c,\perp}(H)$ for crystals $Pr_xY_{1-x}Fe_3(BO_3)_4$ ($x = 1$, 0.75, 0.67, 0.55, 0.45, 0.25) for **H**||**c** (a) and **H** ⊥ **c** (b) at $T = 2$ K. The data for $YFe_3(BO_3)_4$ were taken from [15].

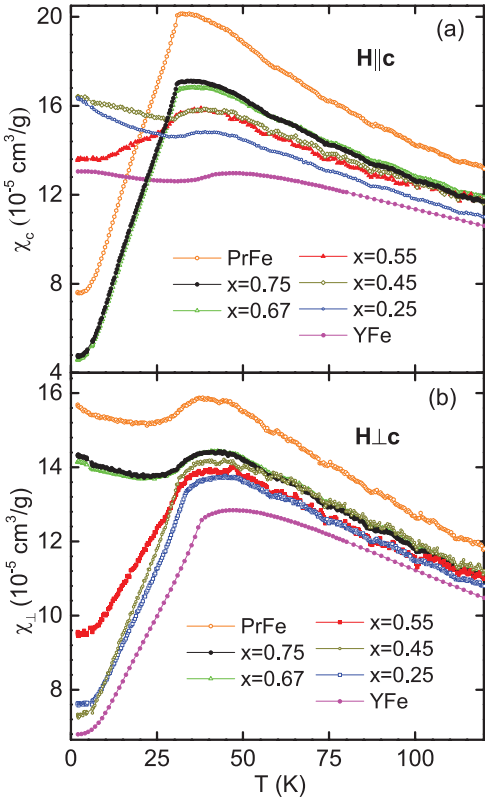

Figure 2. Experimental temperature dependences of the initial magnetic susceptibility $\chi_{c,\perp}(T)$ for crystals $Pr_xY_{1-x}Fe_3(BO_3)_4$ ($x = 1$, 0.75, 0.67, 0.55, 0.45, 0.25) for **H**||**c** (a) and **H** ⊥ **c** (b) at $H_{c,\perp} = 1$ kOe. The data for $YFe_3(BO_3)_4$ were taken from [15].

spin-reorientation transition, the initial magnetic susceptibilities for $x = 0.75$ and 0.67 are also less than that of the undiluted crystal.

Most likely this is due to a decrease in the contribution of the Pr subsystem to the magnetic susceptibility of the crystal with diamagnetic dilution. For the same reason, the total magnetic susceptibilities of the crystals with $x = 0.75$ and 0.67 measured in the field of 1 kOe along the trigonal axis (see figure 2) are less than that of the undiluted crystal at all temperatures.

An unusual two-step spin reorientation is found for the samples with $x = 0.75$ and 0.67 if the magnetic field is applied along the trigonal axis (figure 1(a)). The first pronounced jump of the magnetization occurs in the field $H_{SR1} \approx 21.6$ kOe (for $x = 0.75$) or $H_{SR1} \approx 11.2$ kOe (for $x = 0.67$), and then the second jump follows in $H_{SR2} \approx 29$ kOe ($x = 0.75$) or $H_{SR2} \approx 21.7$ kOe ($x = 0.67$). Both the critical fields H_{SR1} and H_{SR2} increase with rising temperature. At $T = 30$ K, close to T_N, the magnetization curves are linear for all compounds (see figure 3(a) for $x = 0.75$ and figure 4(a) for $x = 0.67$).

We know from the neutron data [18] that the compound with $x = 0.55$ has the INC magnetic structure with the magnetic moments of iron being close to equidistant from both the c axis and the basal plane. Therefore, anomalies in the magnetization curves can be seen in both the **H**||**c** and the **H**⊥**c** directions of the field (see figure 5(a)). When magnetizing along the trigonal axis, the jump of the magnetization due to the spin reorientation occurs in the critical field $H_{SR} \approx 8.4$ kOe at $T = 2$ K. The value of the magnetization jump is small at this transition because due to the INC magnetic structure the magnetization along the trigonal axis at $H < H_{SR}$ is determined by a combination of parallel and perpendicular susceptibilities. At the same time, if the magnetization is in the basal plane, the magnetization behavior is typical of EP structures with a 120° domain structure [20]. The magnetization process in fields below 10 kOe is determined by the dynamics of the domain structure, resulting in the nonlinear behavior of the magnetization at $H < 10$ kOe. In the compound with a more diluted Pr subsystem ($x = 0.45$) the magnetization curves only show anomalies for **H** ⊥ **c** (see figure 6(a)) with linear magnetization curves at **H**||**c** for all $T < T_N$.

The $Pr_{0.25}Y_{0.75}Fe_3(BO_3)_4$ crystal with the most diluted Pr subsystem shows magnetization curves that are typical of EP antiferromagnets, and these are closest to the dependences of the EP $YFe_3(BO_3)_4$ single crystal (see figures 1 and 7(a)).

The study of the gradual transformation of the magnetic structure in the family of $Pr_xY_{1-x}Fe_3(BO_3)_4$ single crystals with a wide set of dilution parameters can be also made using analyses of the curves for magnetic susceptibilities $\chi_{c,\perp}(T)$ at temperatures $T < T_N$. As for the magnetization curves, the magnetic susceptibilities $\chi_{c,\perp}(T)$ at temperatures $T < T_N$ for $x = 0.25$ are close to those of the EP antiferromagnet $YFe_3(BO_3)_4$. With growing x, the contribution of the Pr subsystem to the anisotropy increases and promotes the transformation of the initial magnetic state to a more pronounced INC phase in which the magnetic moments of iron are located

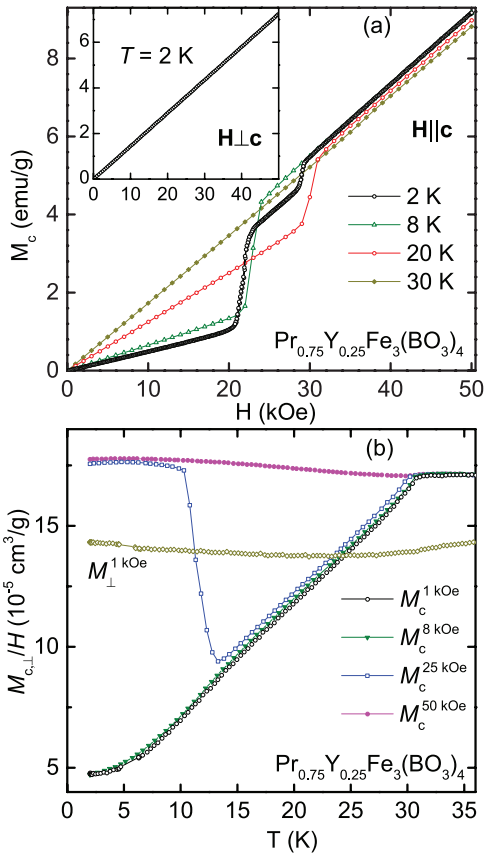

Figure 3. Experimental magnetizing curves $M_{c,\perp}(H)$ for **H**||**c** and **H** $\perp$ **c** (inset) at the indicated temperatures (a) and temperature dependences of the normalized magnetization $M_{c,\perp}/H$ for $T < T_N$ at the indicated fields (b) for $Pr_{0.75}Y_{0.25}Fe_3(BO_3)_4$.

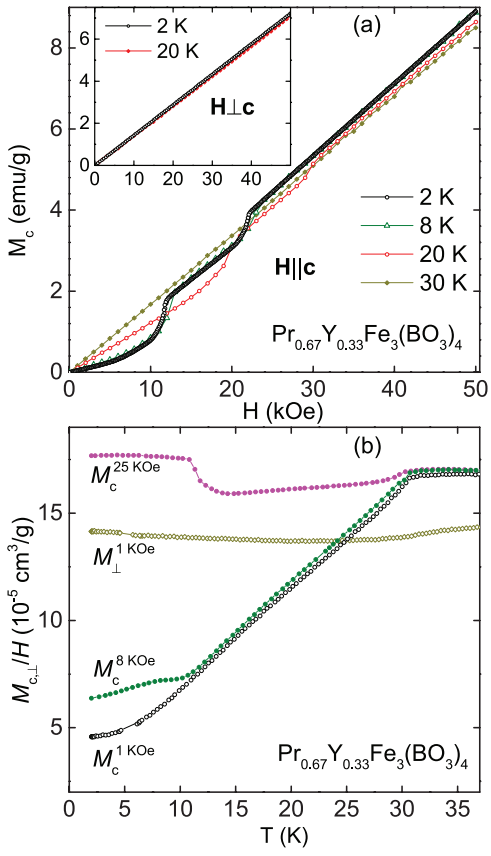

Figure 4. Experimental magnetizing curves $M_{c,\perp}(H)$ for **H**||**c** and **H** $\perp$ **c** (inset) at the indicated temperatures (a) and temperature dependences of the normalized magnetization $M_{c,\perp}/H$ for $T < T_N$ at the indicated fields (b) for $Pr_{0.67}Y_{0.33}Fe_3(BO_3)_4$.

ever closer to the c axis when x increases. As a result, the curves $\chi_{c,\perp}(T)$ for $x = 0.75$ almost do not differ from the similar dependences of the EA antiferromagnet $PrFe_3(BO_3)_4$. A strong correlation between the parameter x and the susceptibility behavior also persists in the paramagnetic range $T > T_N$, where the susceptibilities $\chi_{c,\perp}(T)$ increase with growing x because of the increasing contribution of the Pr subsystem. The exception found for the compound with $x = 0.45$ is likely due to high systematic errors, since the measurements in this case were made on the sample with the smallest size.

Figures 3(b), 4(b) and 5(b) show the curves $M_{c,\perp}(T)/H$ where the magnetization has been normalized by the respective measuring field. Some of the curves $M_c(T)$ show unusually sharp jumps of the magnetization at some temperature $T < T_N$ (see e.g. the curve for 25 kOe in figure 3(b)). A comparison of these curves with the field dependences of the magnetization measured at different temperatures allows us to assert that these jumps are observed when the strength of the magnetic field applied is close to the critical fields of the spin reorientations H_{SR} and that they are due to the transition occurring as the temperature changes.

Thus, the changes in the field and temperature dependences of the magnetization in the $Pr_xY_{1-x}Fe_3(BO_3)_4$ family confirm that the magnetic moments of iron tilt closer to the basal plane as the praseodymium content is reduced. This fact is illustrated in figure 8, which shows how the inclination of the magnetic moments of the Fe subsystem relative to the basal plane changes from 90° for $x = 1$ to 0° for $x = 0$ over intermediate values as a function of x. This graph uses results from neutron research data[4] [8, 10, 18], apart from the compounds with $x = 0.75$ and 0.25, whose magnetic structures have not been verified by neutron diffraction. It is not possible to establish precise boundaries between the EP, INC and EA states. We note, however, that the magnetic data indicate a full EP state for the $x = 0.25$ compound, and the AFMR data confirm an INC type magnetic structure for the crystal with $x = 0.75$.

The concentration dependence of the Neel temperature is also shown in figure 8.

Figure 9 shows the frequency-field dependences of the AFMR measured in the magnetic fields **H**||**c** at $T = 4.2$ K for three compounds with $x = 1$, 0.75 and 0.67. Since the energy gaps of the AFMR ω_c of all the compounds differ strongly, the dependences are shown in normalized form: the resonance frequencies are divided by the appropriate value of the critical frequency ω_c, which is measured for every compound at $T = 4.2$ K. Similarly, the resonance fields are divided by ω_c/γ, where γ is the gyromagnetic ratio. The solid and dotted lines in the figure are the theoretical frequency-field dependences calculated for an EA antiferromagnet in the states before and after the SF transition, respectively [21]. It can be seen that the frequency-field dependences of $PrFe_3(BO_3)_4$, which has an EA antiferromagnetic structure, are quite satisfactorily described

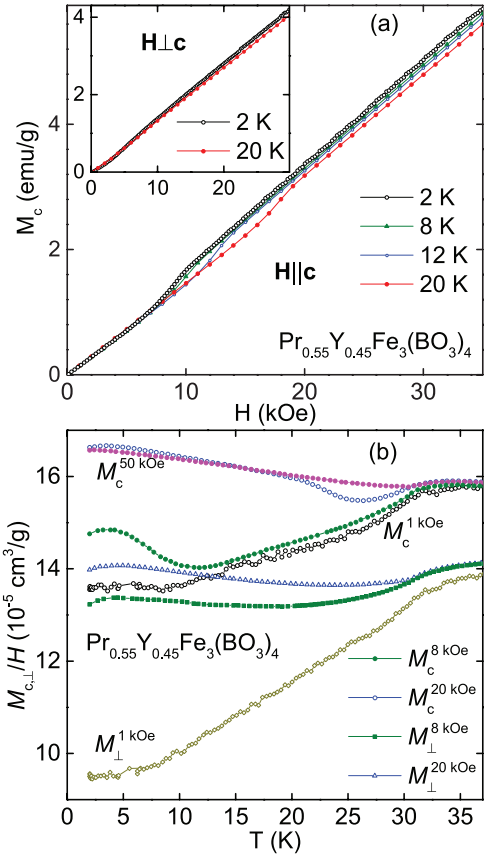

Figure 5. Experimental magnetizing curves $M_{c,\perp}(H)$ for **H**||**c** and **H** ⊥ **c** (inset) at the indicated temperatures (a) and temperature dependences of the normalized magnetization $M_{c,\perp}/H$ for $T < T_N$ at the indicated fields (b) for $Pr_{0.55}Y_{0.45}Fe_3(BO_3)_4$.

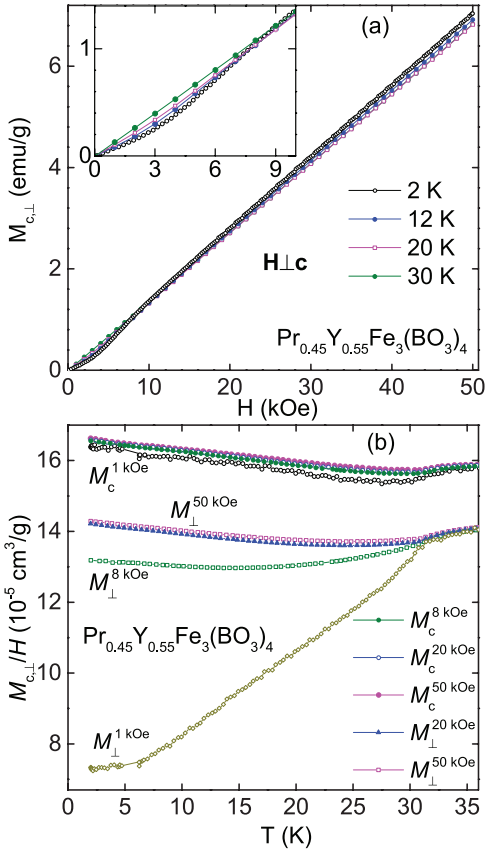

Figure 6. Experimental magnetizing curves $M_{c,\perp}(H)$ for **H** ⊥ **c** at the indicated temperatures (a) and temperature dependences of the normalized magnetization $M_{c,\perp}/H$ for $T < T_N$ at the indicated fields (b) for $Pr_{0.45}Y_{0.55}Fe_3(BO_3)_4$.

by the theoretical calculation. In particular, the oscillations in the SF state appear in magnetic fields that exceed the critical field of the SF transition corresponding to $H_{norm} \approx 1$.

By contrast, the spin reorientation in the $Pb_{0.67}Y_{0.33}Fe_3(BO_3)_4$ compound with an INC structure starts at the field H_{SR1}, marked in this plot by the left blue arrow, which is below the expected ω_c/γ value (the right blue arrow corresponds to the field H_{SR2}). Furthermore, the experimental frequency-field dependence differs strongly from that calculated for the EA state.

The resonance data for the compound with $x = 0.75$ are intermediate between those of $x = 1.0$ and 0.67 and suggest that the magnetic structure of this compound is also the INC one, but with magnetic moments that are closer to the c axis than is the case in $Pb_{0.67}Y_{0.33}Fe_3(BO_3)_4$. Detailed information concerning the AFMR in the $Pr_xY_{1-x}Fe_3(BO_3)_4$ family of single crystals will be presented elsewhere.

4. Theory

The magnetic properties of $Pr_xY_{1-x}Fe_3(BO_3)_4$ crystals are determined by both the magnetic subsystems and the interaction between them. The Fe subsystem in this compound can be considered as consisting of two antiferromagnetic sublattices. The R subsystem (magnetized due to the *f–d* interaction) can also be represented as a superposition of two sublattices. In the calculations, we use a theoretical approach that has been applied for the description of the magnetic properties of $RFe_3(BO_3)_4$ compounds (see e.g. [2, 14, 22, 23]). This approach is based on a crystal-field model for the R ion and the molecular-field approximation. Effective Hamiltonians that describe the interaction of each R/Fe ion in the ith ($i = 1, 2$) sublattice of the corresponding subsystem in the applied magnetic field **H** can be written as

$$\mathcal{H}_i(\mathrm{Pr}) = \mathcal{H}_i^{\mathrm{CF}} - g_J\mu_B\mathbf{J}_i\,[\mathbf{H}+\lambda_{fd}\mathbf{M}_i^{\mathrm{Fe}}]\,, \tag{1}$$

$$\mathcal{H}_i(\mathrm{Fe}) = -g_S\mu_B\mathbf{S}_i\,[\mathbf{H}+\lambda\mathbf{M}_j^{\mathrm{Fe}} + x\lambda_{fd}\mathbf{m}_i^{\mathrm{Pr}}]\,, \quad j = 1, 2,\ j \neq i, \tag{2}$$

where $\mathcal{H}_i^{\mathrm{CF}}$ is the crystal-field Hamiltonian, g_J is the Lande factor, $\mathbf{J}_i$ is the operator of the angular moment of the R ion, $g_S = 2$ is the g value, $\mathbf{S}_i$ is the operator of the spin moment of an iron ion and $\lambda_{fd} < 0$ and $\lambda < 0$ (including intrachain $\lambda_1 < 0$ and interchain $\lambda_2 < 0$) are the molecular constants of the antiferromagnetic interactions R–Fe and Fe–Fe, respectively. Note that the molecular constant λ_{fd} only describes the isotropic *f–d* exchange interaction. The magnetic moments of the ith iron $\mathbf{M}_i^{\mathrm{Fe}}$ and rare-earth $\mathbf{m}_i^{\mathrm{Pr}}$ sublattices per formula unit are defined as

$$\mathbf{M}_i^{\mathrm{Fe}} = 3g_S\mu_B\langle\mathbf{S}_i\rangle, \quad \mathbf{m}_i^{\mathrm{Pr}} = g_J\mu_B\langle\mathbf{J}_i\rangle. \tag{3}$$

The right part of the equation for $\mathbf{M}_i^{\mathrm{Fe}}$ is a relevant Brillouin function, as it should be in the case of an equidistant spectrum that is typical for a Fe^{3+} ion with an orbital singlet as a ground state (S ion).

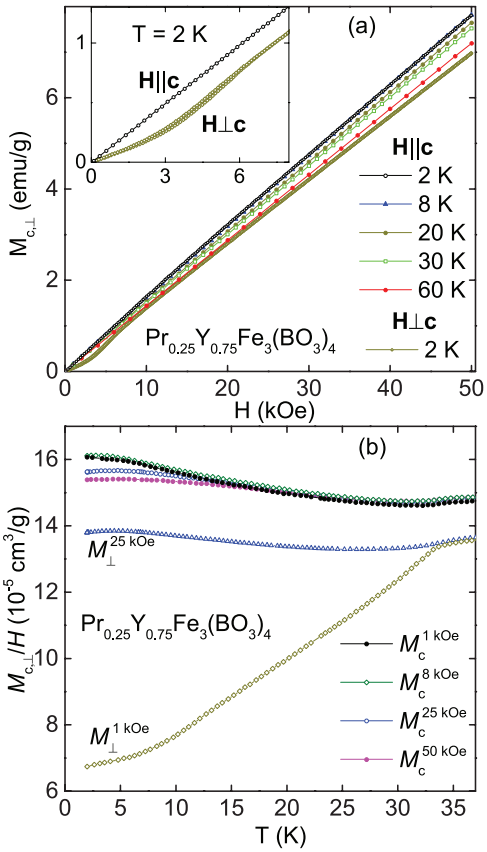

Figure 7. Experimental magnetizing curves $M_{c,\perp}(H)$ for **H**||**c** and **H** ⊥ **c** (inset) at the indicated temperatures (a) and temperature dependences of the normalized magnetization $M_{c,\perp}/H$ for $T < T_N$ at the indicated fields (b) for $Pr_{0.25}Y_{0.75}Fe_3(BO_3)_4$.

The crystal-field Hamiltonian $\mathcal{H}^{CF}$ can be expressed using the irreducible tensor operators C_q^k as

$$\mathcal{H}^{CF} = B_0^2 C_0^{(2)} + B_0^4 C_0^{(4)} + iB_{-3}^4 (C_{-3}^{(4)} + C_3^{(4)}) + B_0^6 C_0^{(6)} + iB_{-3}^6 (C_{-3}^{(6)} + C_3^{(6)}) + B_6^6 (C_{-6}^{(6)} + C_6^{(6)}). \quad (4)$$

For the Pr^{3+} ion in $Pr_xY_{1-x}Fe_3(BO_3)_4$ ($x = 0.75$, 0.67, 0.55, 0.45, 0.25), the crystal-field parameters B_q^k are unknown and data on the splitting of the ground-state multiplet are unavailable. As the environment of the rare-earth ion depends on x, the parameters of the crystal field for different compounds should be slightly different.

In order to calculate the magnitudes and orientations of the magnetic moments in the Fe and R subsystem s, it is necessary to solve a self-consistent problem based on Hamiltonians (1) and (2) under the condition of the minimum for the corresponding thermodynamic potential (see e.g. [2, 20, 22]) for the given temperature and field. Then it is possible to determine the regions of stability of various magnetic phases, the critical fields for the phase transitions, the magnetization curves, the magnetic susceptibilities, etc.

The anisotropy energy for the ith sublattice of the Fe subsystem for a crystal of trigonal symmetry can be written as

$$\Phi_{an}^i = K_2^{Fe} \cos^2\theta_i + K_4^{Fe} \cos^4\theta_i + K_{66}^{Fe} \cos^6\theta_i \cos 6\varphi_i, \quad (5)$$

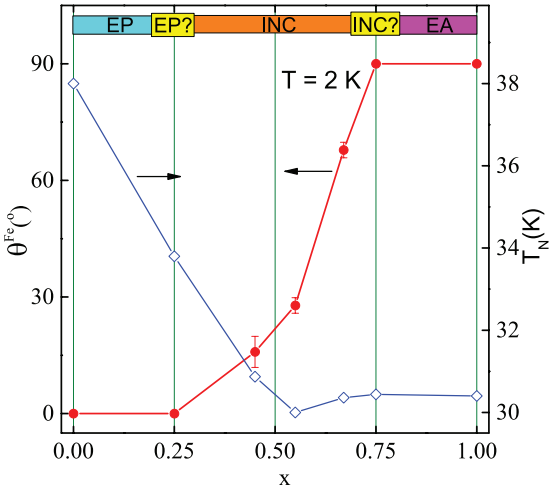

Figure 8. Inclination angle of the Fe moments relative to the hexagonal basal plane at $T = 2$ K and the Neel temperature as functions of x in $Pr_xY_{1-x}Fe(BO_3)_4$ ($x = 1$, 0.75, 0.67, 0.55, 0.45, 0.25, 0).

where an anisotropy constant $K_2^{Fe} < 0$ stabilizes the EP state, a constant $K_4^{Fe} > 0$ stabilizes the EA state, $K_{66}^{Fe} < 0$ is the anisotropy constant in the basal ab plane and θ_i and φ_i are the polar and azimuth angles of the magnetic moment $\mathbf{M}_i^{Fe}$ of iron, respectively.

The magnetization and magnetic susceptibility of the compound (per f.u.) are defined as

$$\mathbf{M} = \frac{1}{2}\sum_{i=1}^{2}(\mathbf{M}_i^{Fe} + x\mathbf{m}_i^{Pr}), \quad \chi_k = \chi_k^{Fe} + x\chi_k^{Pr}, \; k = a, b, c. \quad (6)$$

In the ordered phase, the initial magnetic susceptibility of the compound under consideration can be determined using the initial linear portions of the magnetization curves calculated for the corresponding directions of the external magnetic field. In the paramagnetic phase where the interactions between rare-earth and iron subsystems can be ignored, the magnetic susceptibility of the rare-earth subsystem can be determined using the well-known Van Vleck formula for the energy spectrum and wave functions calculated on the basis of the crystal-field Hamiltonian (4). For the Fe subsystem, the susceptibility can be described in terms of the Curie–Weiss law (with the corresponding value of the paramagnetic Neel temperature Θ).

5. Comparison of experimental data and theoretical calculations

In order to determine the parameters B_q^k of a crystal-field forming the electronic structure of a rare-earth ion, we used the experimental data for the temperature dependence of the magnetic susceptibility $\chi_{c,\perp}(T)$ and existing information on the structure of the ground multiplet of Pr^{3+} ion in $PrFe_3(BO_3)_4$ [24]. The parameters determined earlier for pure $PrFe_3(BO_3)_4$ [23, 24] and other EA [2] and EP [20] ferroborates were taken as the initial values of the crystal field

parameters from which the procedure for minimization of the corresponding desired function was begun. To determine the sets of parameters B_q^k that can describe the entire set of the measured magnetic characteristics for each of the compounds of $Pr_xY_{1-x}Fe_3(BO_3)_4$ with different concentrations x, we calculated the magnetization curves along the trigonal axis and in the basal plane $M_{c,\perp}(H, T)$ (at $T = 2$, 8, 12, 20 and 30 K and up to 50 kOe) and determined the parameters λ_1 and λ_2 defining the exchange fields $H_{dd1} = \lambda_1 M_0^{Fe}$ and $H_{dd2} = \lambda_2 M_0^{Fe}$. For the high-field region $H > H_{SR}$, the slope of the magnetization curve $M_{c,\perp}(H)$ is determined by the parameter λ_1 of the intrachain antiferromagnetic Fe–Fe exchange interaction, since it is the main interaction preventing the rotation of the magnetic moments of the iron subsystem in the flop phase toward the field direction. The parameter λ_2 appearing in the Brillouin function is mainly responsible for the value of the magnetic moment of iron at a given temperature and magnetic field and determines the Neel temperature. It was determined from the best agreement between experimental and calculated magnetization curves for all temperatures.

Another important criterion for the final choice of the crystal field parameters is the concordance of the calculated and experimental magnetic moments of praseodymium μ_{exp}^{Pr} at low temperature found in [18] for compounds with $x = 0.67$, 0.55, 0.45 and in [10] [4]for $PrFe_3(BO_3)_4$. Our calculations show that this criterion imposes substantial restrictions on parameters. The calculated magnetic moment of the Pr_x subsystem μ_{calc}^{Pr} depends on the crystal field parameters and the parameter λ_{fd} defining the *f–d* exchange field $H_{fd} = \lambda_{fd} M_0$. For each of the compounds, we defined the parameter λ_{fd} providing the experimental value of μ_{exp}^{Pr} (within experimental error) (see table 1).

The sets of the crystal field parameters B_q^k for $Pr_xY_{1-x}Fe_3(BO_3)_4$ ($x = 0.75 - 0.25$) that were determined by following the criteria that best described the $\chi_{c,\perp}(T)$ and $M_{c,\perp}(H, T)$ curves and the values of μ_{exp}^{Pr} are listed in table 1. These parameters were determined based on the ground multiplet; therefore, they can only be considered as effective parameters suitable for describing the thermodynamic properties of the compound. The set of the crystal field parameters corresponding to the energies of the six lower levels of the ground multiplet of the Pr^{3+} ion in $Pr_xY_{1-x}Fe_3(BO_3)_4$ ($x = 0.75$, 0.67, 0.55, 0.45, 0.25) are given in table 1 for $H = 0$. These energies were determined for both $T = 50\,K > T_N$ and $T = 3\,K$, where the *f–d* interaction was taken into consideration, resulting in the removal of the degeneracy of the lower levels.

In our previous paper [18] a single set of parameters of the crystal field of the pure EA compound $PrFe_3(BO_3)_4$ was used for three compounds with $x = 0.67$, 0.55, 0.45 to obtain the exchange and anisotropy parameters. As a development of this approach, the parameters defining the magnetic properties of every compound in the family $Pr_xY_{1-x}Fe_3(BO_3)_4$ were determined in this study using both the broader basis of the experimental data and the set of parameters of the crystal field specified for every compound. Therefore, the parameters presented here in table 1 are more reliable than those given in [18]. Table 1 also shows the parameters for pure $PrFe_3(BO_3)_4$, which were determined from the experimental data and using the crystal field parameters found solely for this crystal in [24]. The closeness of the values of H_{dd1}, H_{dd2} and H_{fd} obtained for all the compounds (including $PrFe_3(BO_3)_4$) is evidence that reasonable crystal field parameters were determined here for the compounds with $x = 0.75 \div 0.25$.

In the calculations, we also used the uniaxial anisotropy constants of iron (K_2^{Fe} and K_4^{Fe}) and the anisotropy constant of iron in the basal plane (K_{66}^{Fe}) from equation (5). The low-temperature constants K_2^{Fe} and K_4^{Fe} were determined for compounds with $x = 0.67$, 0.55 and 0.45 by matching the calculated and experimental values of the inclination angle of the Fe moment from the basal plane θ_{exp}^{Fe}, which are known from the neutron data [18]. Since the θ_{exp}^{Fe} experimental data omit $x = 0.25$ and 0.75, the anisotropy constants K_2^{Fe} and K_4^{Fe} used for $x = 0.25$ were those of $x = 0.45$, representing the compound with the closest composition for which the magnetic structure had been determined by neutron diffraction. For the compound with $x = 0.75$, it was possible to estimate constants when describing the curves $\chi_{c,\perp}(T)$ using those for $x = 0.67$ as the initial ones. Then, with the chosen parameters (λ_1, λ_2 and λ_{fd}), we fitted the temperature dependences of the constants K_2^{Fe} and K_4^{Fe}, which decrease with temperature and describe the main features of the experimental dependences $\chi_{c,\perp}(T)$. It can be seen that the values of the anisotropy constants K_2^{Fe} and K_4^{Fe} of the iron ions, which are determined with individual sets of crystal field parameters for each compound (table 1), are noticeably smaller than those found in [18]. In particular, use of the crystal field parameters of $PrFe_3(BO_3)_4$ [24] with EA anisotropy resulted in [18] in exaggerated values of K_2^{Fe}. Note that the values of the anisotropy constant K_2^{Fe} obtained for the compounds with $x = 0.45$ and 0.25 are close to that of the net $YFe_3(BO_3)_4$. It is important that the EA and EP states (in $PrFe_3(BO_3)_4$ and $YFe_3(BO_3)_4$, respectively) can be described using only the anisotropy constant K_2^{Fe}, but the description of the INC state requires both K_2^{Fe} and K_4^{Fe} constants. Thus, the anisotropy constant K_4^{Fe} plays an important role in stabilizing the INC state.

As an anisotropy constant K_2^{Fe} for the pure compound $PrFe_3(BO_3)_4$, a value is taken that corresponds to the resulting anisotropy field for the closest composition with $x = 0.75$, whose anisotropy is determined by two constants K_2^{Fe} and K_4^{Fe}.

Table 1 shows that a significant reduction of μ^{Pr}, both calculated and measured, takes place as the parameter x decreases. This has to be related to the fact that the magnetic moment μ^{Pr} in the EA, INC and EP states depends on the splitting of the lowest energy levels of the Pr ion. Due to the *f–d* exchange interaction, the Pr subsystem adds the EA contribution to the total magnetic anisotropy of the crystal. As the diamagnetic dilution increases with decreasing x, the magnetic moments of the iron ions tilt progressively towards the basal plane. At the same time, the magnetic moments of the ions Pr^{3+} which are connected with the iron moments by the *f–d* interaction tilt more to the basal plane, thereby reducing the splitting of the lowest energy levels of Pr^{3+} and leading to a reduction of the magnetic moment μ^{Pr}.

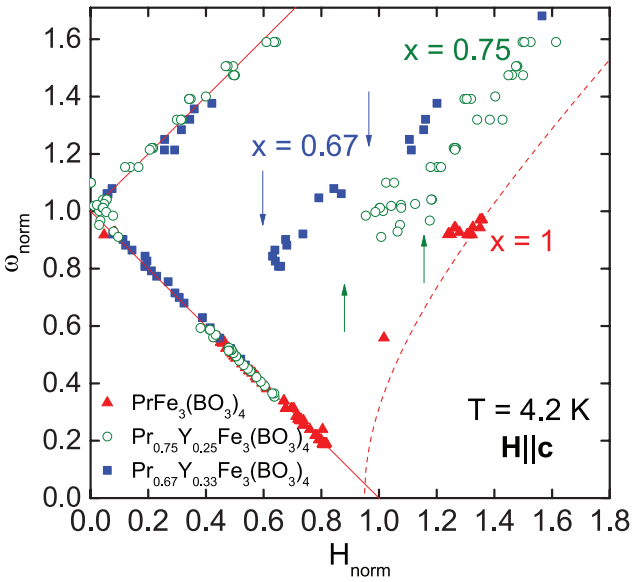

Figure 9. Frequency-field dependences of AFMR at $T = 4.2$ K and **H**||**c** in $Pr_xY_{1-x}Fe(BO_3)_4$ ($x = 1$, 0.75, 0.67).

The value of the magnetic moment on the Fe site for the doped compounds stays nearly constant with $\mu^{Fe} \approx 4.2$–4.5 μ_B and has a similar moment value to that found in pure $PrFe_3(BO_3)_4$, where $\mu^{Fe} = 4.3$ μ_B, or $YFe_3(BO_3)_4$, with $\mu^{Fe} = 3.95$ μ_B (see table 1). The value of the magnetic moment per Pr ion changes from $\mu^{Pr} = 0.8(1)$ μ_B in $x = 1$ to $\mu^{Pr} = 0.8(3)$ μ_B for $x = 0.67$ and $\mu^{Pr} = 0.4(4)$ μ_B for $x = 0.55$ before it becomes too small to be detectable by neutron diffraction in the $x = 0.45$ compound. It is noteworthy that in this last compound the influence of the strongly diluted Pr sublattice is nevertheless still visible through the non-planar component μ_z^{Fe}. The magnetic transition temperature for $1.0 \leqslant x \leqslant 0.25$ remains constant at $T_N \approx 30$–34 K, noticeably below the $T_N = 38$ K found for $x = 0$ (figure 8). If the transition temperature followed the dependence on the rare-earth ionic radius exactly, as described by Hinatsu *et al* [6], one would have expected T_N to increase to about 36 K in $Pr_{0.25}Y_{0.75}Fe_3(BO_3)_4$.

The theoretical dependences presented below in the figures were calculated using the parameters given in the table 1. In the calculation for each x value, all the experimental data for this compound were considered simultaneously, and the sensitivity of the individual experimental dependences to the given parameters was analyzed. To calculate the magnetic characteristics of $Pr_xY_{1-x}Fe_3(BO_3)_4$ when the external magnetic field is directed along the trigonal c axis or perpendicular to it, we used the schemes of orientation of the magnetic moments of the iron $\mathbf{M}_i^{Fe}$ and rare-earth $\mathbf{m}_i^{Pr}$ subsystems shown in figure 10. The schemes in figures 10(a) and (b) were used for the case of $H = 0$ (cone of easy magnetization axes—INC state (a) and EA state (b)). The calculations according to the schemes in figures 10(c) and (d) were performed for a field directed along the trigonal axis (**H**||**c**). The schemes in figures 10(e) and (f) were used for the case of a magnetic field oriented in the basal plane (**H** ⊥ **c**). The scheme in figure 10(e) shows the projections of

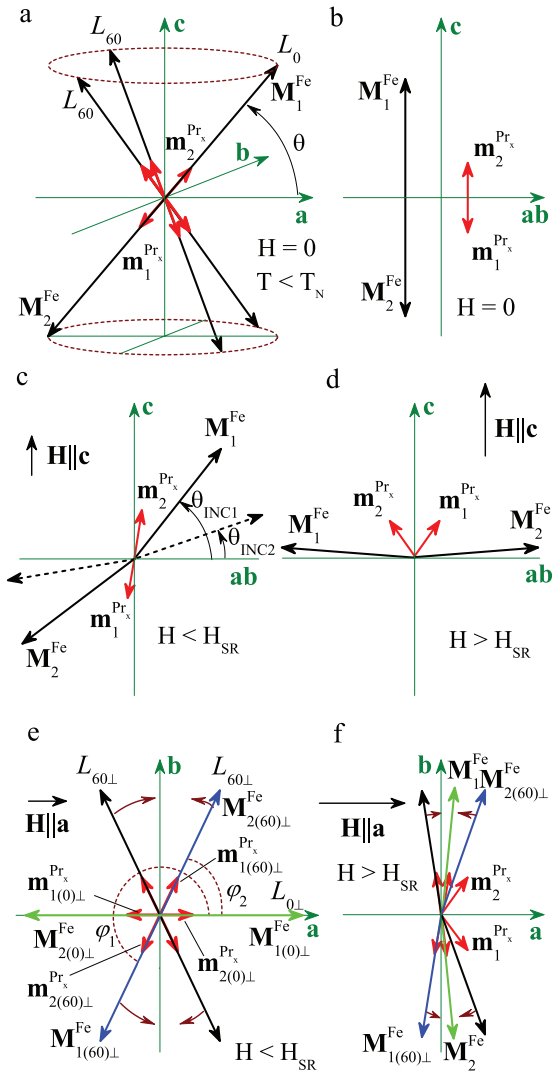

Figure 10. Schemes of the orientations of the magnetic moments of the iron $\mathbf{M}_i^{Fe}$ and praseodymium $\mathbf{m}_i^{Pr}$ subsystems used in the calculation of the magnetic characteristics of $Pr_xY_{1-x}Fe_3(BO_3)_4$ for different directions of the external magnetic field: (a) $H = 0$ (INC state, cone of easy magnetization axes); (b) $H = 0$ (EA state); (c) and (d) **H**||**c** (the basal plane is perpendicular to the figure plane); and (e) and (f) **H** ⊥ **c** (the axis c is perpendicular to the figure plane).

the magnetic moments of the iron ($\mathbf{M}_{iab}^{Fe}$) and rare-earth ($\mathbf{m}_{iab}^{Pr}$) subsystems onto the ab plane in domains with the antiferromagnetic vector $\boldsymbol{L}$ making angles $\varphi_i = 0$ (L_0) and $\varphi_i = \pm 60°$ (L_{60}) relative to the a axis.

5.1. Magnetizing along the c axis

Since the compound with $x = 0.75$ had not been studied by neutron diffraction, its exact magnetic state is not known. The calculations offer a good description of the experimental magnetization curves (at $T = 2$ K and $H < 20$ kOe) and the magnetic susceptibility (at $T < 5$ K and $H < 1$ kOe) assuming either an EA phase ($\theta^{Fe} = 90°$) or an INC state with an inclination angle $80° < \theta^{Fe} < 90°$. Taking into account that the resonance data at $T = 4.2$ K point strongly to the existence of

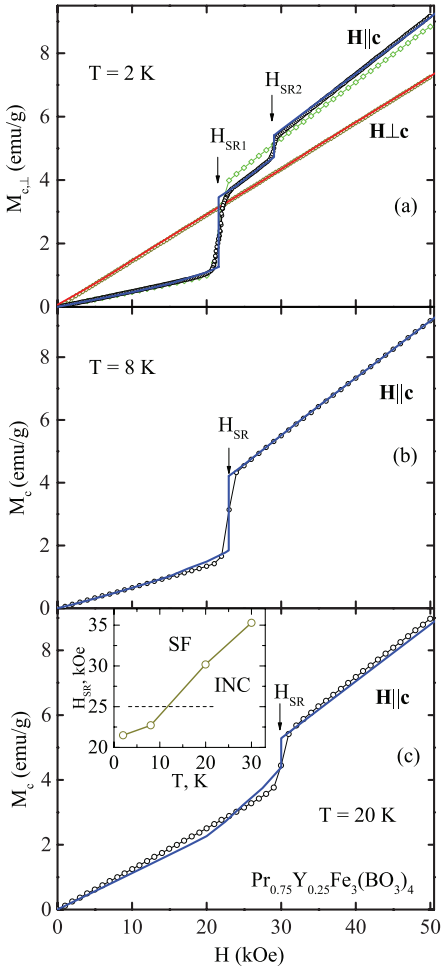

Figure 11. Experimental (symbols: green (a) and black (b), (c) for the quenched sample and black (a) for the unquenched one) and calculated (lines) magnetizing curves for $Pr_{0.75}Y_{0.25}Fe_3(BO_3)_4$ for **H**||**c** and **H** ⊥ **c** at $T = 2$ K (a) and **H**||**c** at $T = 8$ (b) and 20 K (c). The inset shows the temperature dependence of the critical field for the quenched sample.

an INC structure, the calculations were carried out for such a state with $\theta^{Fe} = 85°$ at $T = 3$ K (scheme in figure 10(c)).

The most interesting of the experimental magnetization curves have two magnetization jumps (see figures 11(a) and 12). Various possible origins for such a two-step reorientation were taken into consideration, leading to the idea of the existence of some interjacent INC state which is stable in the range of magnetic fields between H_{SR1} and H_{SR2}. The first, more pronounced, jump of the magnetization at $H = H_{SR1}$ is caused by the reorientation from the zero field INC state (scheme a in figure 10) into the interjacent INC one with an inclination angle θ^{Fe} that is smaller than that in the initial state. The second jump at the field $H = H_{SR2}$ is associated with the reorientation into the flop state (scheme d) and is accompanied by the respective predominant alignment of the Pr moments of both sublattices in the field direction **H**||**c**.

The interjacent INC state arises in some range of magnetic fields due to competition between the Zeeman energy and the magnetic anisotropy of the crystal which, in turn, is formed by the competing Fe and Pr contributions. When the growing field **H**||**c** reaches some critical value H_{SR1} the energy balance achieved in weak fields is broken, resulting in the reorientation into the new INC state with another inclination angle θ^{Fe} being stable in some range of the field until the reorientation into the flop state occurs at $H = H_{SR2}$. As the calculation shows, the values of these angles are close for $x = 0.75$ and 0.67 and are equal to $\theta^{Fe} \approx 23°$ at temperatures $T = 2 - 20$ K.

Note that in our previous work [18] we presented magnetization curves for $Pr_{0.67}Y_{0.33}Fe_3(BO_3)_4$ at $T = 2$ and 8 K which showed only one jump (at $H_{SR} \approx 11.5$ kOe, coinciding with H_{SR1} at $T = 2$ K), in contrast to the two jumps depicted here in figures 1(a) and 4(a). The reason for this is that there were two kinds of samples with $x = 0.67$ at our disposal. Crystals of the first type were cooled after the end of the crystallization process to room temperature at a high rate and were likely quenched. They show only the low-field jump in the field dependence of magnetization, while the high-field one (at $H \approx H_{SR2}$) is only slightly pronounced or completely absent. Just such data were presented in [18]. This paper presents data for samples of the second type, which were cooled slowly to room temperature and experienced two-step spin reorientation, forming the interjacent state. Comparison of the data shows that the critical field of the reorientation in the quenched sample coincides with the H_{SR1} of the unquenched one. Apparently, inhomogeneous strain arising in the quenched samples provides the additional contribution to the anisotropy energy and changes the energy balance required for the formation of the interjacent INC phase, which can only be stabilized at a definite interval of ratios between the first and second anisotropy constants of a crystal. As a result, the spin reorientation occurs directly into the flop state, either throughout the crystal or in the greater part of it, which is the most strained. A similar situation is observed in the samples with $x = 0.75$; figure 11 shows the field dependence of the magnetization of the quenched sample with the conventional one-step spin reorientation at **H**||**c**. We carried out additional measurements solely for the unquenched sample with $x = 0.75$ at $T = 2$ K and found two well-defined magnetization jumps (see black symbols in figure 11(a)), in contrast to the single jump in the quenched one (green symbols).

The two-step character of the spin reorientation of the magnetization $M_c(H)$ in the compounds with $x = 0.75$ and 0.67 prompted us to analyze the magnetization curve of the $PrFe_3(BO_3)_4$ single crystal more carefully. In [17] the field dependence $M_c(H)$ had only been measured at $T = 2$ K in a steady magnetic field up to 50 kOe, leaving room for the speculation that a second jump could occur above this limit. Even though a measurement in pulse magnetic fields up to 80 kOe had also been performed at $T = 4.2$ K in [17], revealing only one jump, a doubt still persists, as the pulse method is substantially less sensitive than the steady-field method, and a small jump of the magnetization could be indiscernible in this case.

Therefore we measured the field dependence of the magnetization of a $PrFe_3(BO_3)_4$ single crystal using a PPMS-6000 in magnetic fields up to 90 kOe directed along the rhombohedral c axis at $T = 2$ K. The curve depicted in the inset of figure 1(a) shows the standard one-step SF transition. These data, together with the temperature dependence of the magnetic susceptibility (also determined using a PPMS-6000), were used to find the set of parameters for $PrFe_3(BO_3)_4$ given in table 1. The absence

Table 1. Parameters for $Pr_xY_{1-x}Fe_3(BO_3)_4$: the intrachain Fe–Fe exchange field H_{dd1}, the interchain Fe–Fe exchange field H_{dd2} and the *f*–*d* exchange field H_{fd} are the low-temperature exchange fields corresponding to the molecular constants λ_1, λ_2 and λ_{fd}, respectively; M^{Fe} is the magnetic moment of the iron per formula unit; $\mu^{Pr}_{calc}/\mu^{Pr}_{exp}$ are the calculated/experimental magnetic moments of praseodymium ($\mu^{Pr}_{calc} = xm^{Pr}$); K_2^{Fe}, K_4^{Fe} and K_{66}^{Fe} are the uniaxial anisotropy constants; H_{SR} is the spin-reorientation transition field; $\theta^{Fe}_{1\,calc}$ is the inclination angle of $\mathbf{M}_1^{Fe}$ relative to the basal plane; T_N is the Neel temperature; Θ is the paramagnetic Neel temperature; Δ—the energies of the six lower levels of the ground multiplet of the Pr^{3+} ion in $Pr_xY_{1-x}Fe_3(BO_3)_4$ at $H = 0$, which are split by the crystal field in the paramagnetic and ordered (with consideration for the *f*–*d* interaction) into temperature ranges; and B_q^k are the parameters of a crystal field.

		$YFe_3(BO_3)_4$	$Pr_xY_{1-x}Fe_3(BO_3)_4$					$PrFe_3(BO_3)_4$	
								$x = 1$	
		$x = 0$	$x = 0.25$	$x = 0.45$	$x = 0.55$	$x = 0.67$	$x = 0.75$	This paper	Other publications
$H_{dd1} = \lambda_1 M_0^{Fe}$, kOe		435	441.6	440	495.7	423.3	442.2	432	
λ_1, kOe/μ_B		–36.3	–35.1	–34.9	–36.7	–33.6	–34.3	–33.5	
$H_{dd2} = \lambda_2 M_0^{Fe}$, kOe		270	286	286	287	288	288	290	
λ_2, kOe/μ_B		–22.5	–22.7	–22.7	–21.3	–22.9	–22.3	–22.5	
$H_{fd} = \lambda_{fd} M_0^{Fe}$, kOe			103.6	118.4	133	135	142.1	115	115 [17], 90–120 [24], 117 [25]
λ_{fd}, kOe/μ_B			–8.2	–9.5	–9.85	–10.7	–11	–8.9	
$M^{Fe} = 3\mu^{Fe}_{exp}$, μ_B		3 · 3.95(5)	3 · 4.2	3 · 4.2	3 · 4.5	3 · 4.2	3 · 4.3	3 · 4.30(3)	
$\mu^{Pr}_{calc}/\mu^{Pr}_{exp}$ ($T = 3$ K), μ_B			0.048/–	0.152/–	0.281/0.4(4)	0.666/0.8(3)	0.795/–	0.94/–	0.79(1) [10], 0.8(1) [18]
K_2^{Fe} ($T = 3$ K), kOe · μ_B		–27.49[a]	–39.12	–39.12	–45.54	–54.23	–54.82	–45.15	
K_4^{Fe} ($T = 3$ K), kOe · μ_B		–	6.21	6.21	6.21	7.45	9.67	–	
K_{66}^{Fe} ($T = 4.2$ K), kOe · μ_B		|0.063|[a]				–0.101[b]			
H_{SR} ($T = 2$ K), kOe	**H**||**c**				8.4	11.2, 21.7	21.6, 29	46	45 [17]
	H ⊥ **c**	~5 [15]	4	5.6	2.9				
$\theta^{Fe}_{1\,calc}/\theta^{Fe}_{exp}$, ° ($T = 3$ K, $B = 0$)		0	→0?/–	16/16(4)	27/27(2)	67/67(2)	→85?/–	90	90
T_N, K		~37 [8], ~38 [15]	~34	~31	~30.2	~30.4	~30.5	~30.5	~32 [10, 17, 26]
Θ, K		–133 [15]	–134	–134	–126	–131	–135	–133	–130 [17]
$\Delta = E_i - E_1$, ($i = 6$), cm^{-1}	$T = 50$ K (paramagnetic state)		0, 44.9, 177.2, 177.2, 219.5, 219.5	0, 53.6, 178.1, 178.1, 227, 227	0, 57.6, 185.7, 185.7, 252, 252,	0, 54.1, 184.5, 184.5, 250.1, 250.1	0, 52.8, 185.4, 185.4, 247.3, 247.3	$\Delta^{calc} = 0$, 53.5, 227.7, 227.7, 309.3, 309.3	$\Delta^{exp} = 0$, 48.5, 192, 192, 275, 275 [24]
	Magnetic state		(EP)	(INC)	(INC)	(INC)	(INC)	(EA)	
	$T = 3$ K		0, 44.8, 177.3, 177.8, 220.1, 220.6	0, 53.9, 176.8, 180.5, 227.6, 229.1	0, 58.9, 181.3, 191.8, 253, 254.6	0, 60.3, 175.5, 195.7, 255.1, 256	0, 60.3, 175.9, 196.7, 253, 254.5	0, 58.8, 215.5, 244.4, 306, 318	

(Continued)

Table 1. (*Continued*)

		$YFe_3(BO_3)_4$	$Pr_xY_{1-x}Fe_3(BO_3)_4$					$PrFe_3(BO_3)_4$	
								$x = 1$	
		$x = 0$	$x = 0.25$	$x = 0.45$	$x = 0.55$	$x = 0.67$	$x = 0.75$	This paper	Other publications
B_q^k, cm^{-1}	B_0^2		415	425	537	531	518	556	
	B_0^4		−1249	−1252	−1329	−1314	−1315	−1447	
	B_{-3}^4		992	972	951	955	949	867	
	B_0^6		130	132	166	160	159	534	
	B_{-3}^6		341	333	397	450	436	165	
	B_6^6		495	513	508	517	507	376 [24]	

[a] The value of the anisotropy constant K_2^{Fe} for $YFe_3(BO_3)_4$ is obtained via AFMR [16] using an energy gap $\omega_c/2\pi = 124$ GHz measured at $T = 4.2$ K, $H_{dd1} = 435$ kOe and $M^{Fe} = 3 \cdot 3.95\ \mu_B$. Similarly, the absolute value of the anisotropy constant K_{66}^{Fe} for $YFe_3(BO_3)_4$ is obtained from the AFMR data [16].

[b] This anisotropy constant is determined for the iron subsystem in the EP state of $NdFe_3(BO_3)_4$ from the description of the magnetization curve $M_\perp(H)$, taking into account the iron moment $M^{Fe} = 3 \cdot 4.2\ \mu_B$ and the anisotropy field in the basal plane, which is equal to 8 Oe (see [20]).

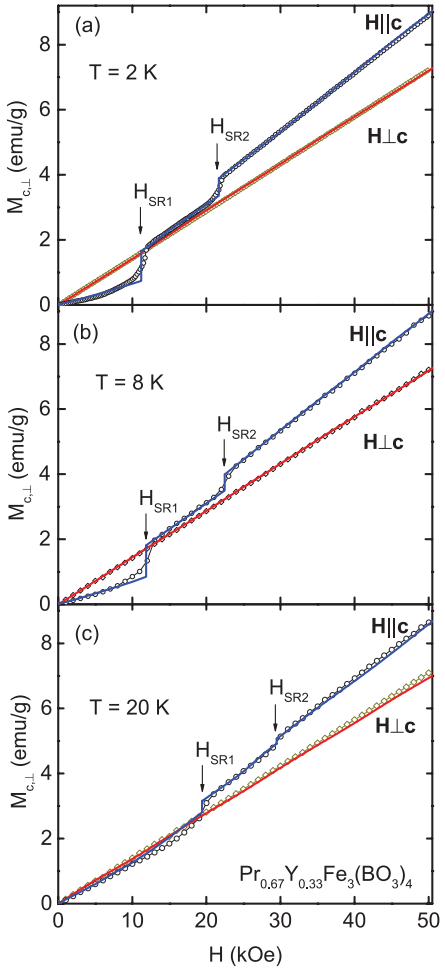

Figure 12. Experimental (symbols) and calculated (lines) magnetizing curves for $Pr_{0.67}Y_{0.33}Fe_3(BO_3)_4$ for **H**||**c** and **H**⊥**c** at $T = 2$ (a), 8 (b) and 20 K (c).

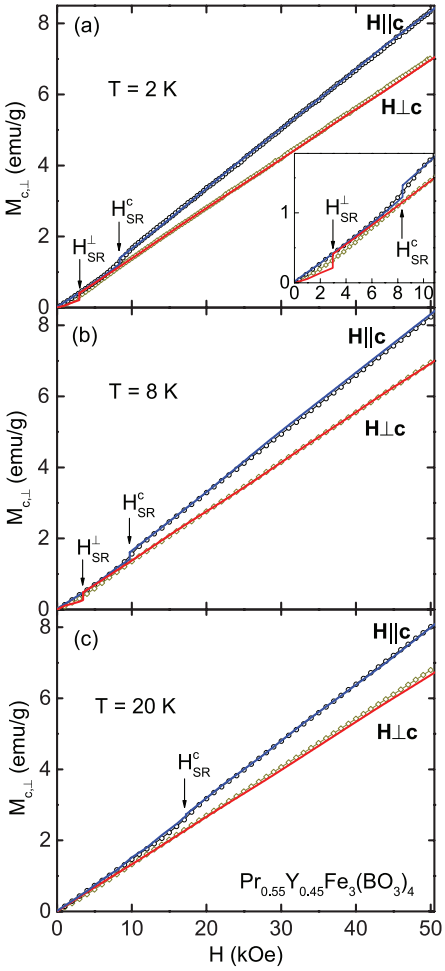

Figure 13. Experimental (symbols) and calculated (lines) magnetizing curves for $Pr_{0.55}Y_{0.45}Fe_3(BO_3)_4$ for **H**||**c** and **H**⊥**c** at $T = 2$ (a), 8 (b) and 20 K (c).

of a second jump of the magnetization in this crystal allows us to suggest that the necessary criterion for the formation of the interjacent INC state at the spin reorientation is a definite relationship between the first and second anisotropy constants for an initial magnetic structure that is INC or very close to it. Such a situation only occurs in the case of $Pr_xY_{1-x}Fe_3(BO_3)_4$ at certain dilutions of the Pr subsystem, including $x = 0.75$ and 0.67.

The resulting magnetization along the c axis is calculated for $x = 0.75 - 0.25$ as follows:

I. In the initial phase for $x = 0.75 - 0.45$ at $H < H_{SR1}$ (INC state, scheme c in figure 10, $\theta_1 = \theta_{INC1}$):

$$M_c = \frac{1}{2}(M_1^{Fe}\cos(\theta_1) + M_2^{Fe}\cos(\theta_2) + m_{2c}^{Pr_x} - m_{1c}^{Pr_x}). \quad (7)$$

II. In the interjacent state for $x = 0.75$ and 0.67 at $H_{SR1} < H < H_{SR2}$ according to equation (7) with $\theta_1 = \theta_{INC2}$ (scheme c).

III. For $x = 0.75$ and 0.67 at $H > H_{SR2}$ (the flop phase) and for $x = 0.55 - 0.25$ (scheme d):

$$M_c = \frac{1}{2}(M_1^{Fe}\cos(\theta_1) + M_2^{Fe}\cos(\theta_2) + m_{2c}^{Pr_x} + m_{1c}^{Pr_x}). \quad (8)$$

Using equations (7) and (8), a good description of the curves $M_c(H)$ is achieved for all the studied ferroborates $Pr_xY_{1-x}Fe_3(BO_3)_4$ ($x = 0.75 \div 0.25$) for all ranges of fields and temperatures (see figures 11–15). For compounds with $x = 0.75$ and 0.67, the calculations of the two-step curves $M_c(H)$ are carried out in three stages, as described above in equations (7) and (8). Figures 11(a) (for $x = 0.75$ at $T = 2$ K) and 12 (for $x = 0.75$ at $T = 2$, 8, 20 K) show that the experimental two-step peculiarities are well described theoretically. The further dilution of the Pr subsystem leads to a strong smoothing of the magnetization jumps on $M_c(H)$ and to the disappearance of the discernible interjacent state because the iron moments are oriented at a small angle to the basal plane even in the initial state. As a result, the INC structures in compounds with $x = 0.55$ (scheme c in figure 10, equation (7)) transform directly into the flop state (scheme d, equation (8)). In the sample with $x = 0.45$, the iron magnetic moments are close to the basal plane ($\theta_{exp}^{Fe} = 16°$ at $T = 3$ K), and there are no anomalies discernible at any temperature in the experimental curves $M_c(H)$ (see figures 13 and 14). For this reason, it appears that the theoretical curves calculated according to equation (8) adequately describe the experimental data in all the measuring ranges of fields and temperatures (see figures 13 and 14). This applies even more to the sample with

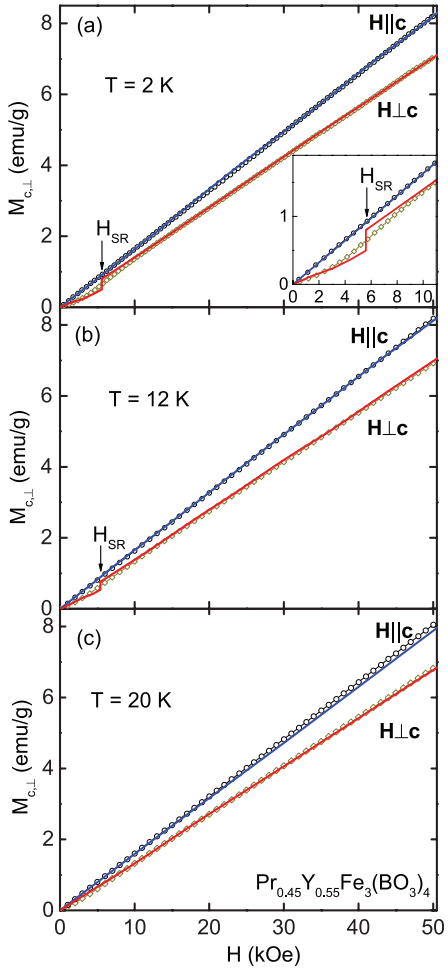

Figure 14. Experimental (symbols) and calculated (lines) magnetizing curves for $Pr_{0.45}Y_{0.55}Fe_3(BO_3)_4$ for **H**||**c** and **H** ⊥ **c** at $T = 2$ (a), 12 (b) and 20 K (c).

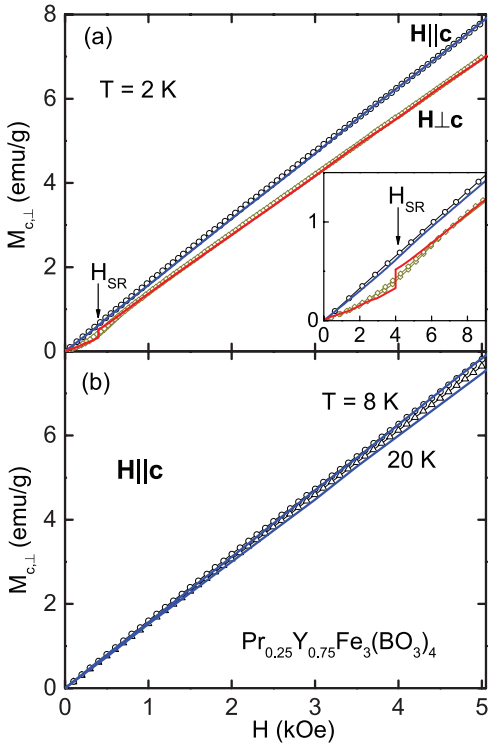

Figure 15. Experimental (symbols) and calculated (lines) magnetizing curves for $Pr_{0.25}Y_{0.75}Fe_3(BO_3)_4$ for **H**||**c** and **H** ⊥ **c** at $T = 2$ K (a) and **H**||**c** at $T = 8$ and 20 K (b).

$x = 0.25$ (figure 15), where the magnetic moments of Fe and Pr lie in the basal plane (scheme d) or very close to it.

5.2. Magnetization in the basal plane

Below the field of saturation of the domain structure (near 10 kOe), a nonlinear behavior of $M_\perp(H)$ is observed, as shown in figures 5(a)–7(a), for $x = 0.55$, 0.45 and 0.25. In the compounds with $x = 0.75$ and 0.67 where the inclination angle of the Fe moments relative to the basal plane is close to $\pi/2$, the magnetization curves $M_\perp(H)$ are linear in all the ranges of magnetic fields and temperatures used (see figures 3 and 4).

A trigonal crystal with magnetic moments lying in the basal plane can contain three types of antiferromagnetic domains, with the antiferromagnetic vectors **L** being oriented along the corresponding twofold axes due to the weak anisotropy in the basal plane. When trigonal $Pr_xY_{1-x}Fe_3(BO_3)_4$ crystals are magnetized in the basal plane *ab* in fields lower than about 10 kOe, all three possible domains with antiferromagnetic axes located at an angle of 120° to each other contribute to the magnetization (see figure 10(e)). The magnetization curves $M_\perp(H)$ were calculated using the approach proposed in [20], where the magnetization processes occurring in EP $NdFe_3(BO_3)_4$ were studied with consideration for the possible existence of three types of domains (see also [22]). Since the information regarding the domain structure of the sample is absent, the domain sizes are assumed to be equal.

During the magnetization in the basal plane for **H**||**a** the magnetic moments of iron in the domain with the antiferromagnetic vector $\boldsymbol{L}_{0\perp}$ directed along the applied field (green vectors $\mathbf{M}^{Fe}_{1,2(0)\perp}$ in figure 10(e)) make a contribution that increases with the field due to an increase in the inclination to the field **H**||**a**. Here $\mathbf{M}^{Fe}_{1,2(0)\perp}$ denote projections of the moments of the antiferromagnetic Fe sublattices $\mathbf{M}^{Fe}_{1,2}$ onto the basal plane in the domain with the antiferromagnetic vector $L_{0\perp}$; similar notations are used for the indices of the Pr moment. In the Pr subsystem, the moment $\mathbf{m}^{Pr_x}_{1(0)\perp}$ is directed opposite to the field direction and decreases with increasing field. As a result, the total magnetization of this domain increases weakly with the field. In the other two domains with the antiferromagnetic vectors $\boldsymbol{L}_{60\perp}$directed at an angle of ±60° to the field (which are equivalent with respect to the direction of **H**||**a**), both the magnetic moments of iron $\mathbf{M}^{Fe}_{1,2(60)\perp}$ in each domain rotate toward the flop state, coinciding with the directions of $\mathbf{M}^{Fe}_{1,2(0)\perp}$ in scheme f. Calculations show that the moment $\mathbf{M}^{Fe}_{1(60)\perp}$ rotates slightly faster than $\mathbf{M}^{Fe}_{2(60)\perp}$. Due to the different rotational speed, the total contribution of these domains to the total magnetization increases with the field.

The total magnetization for a field **H**||**a**, $H < H_{SR}$ (scheme e in figure 10)

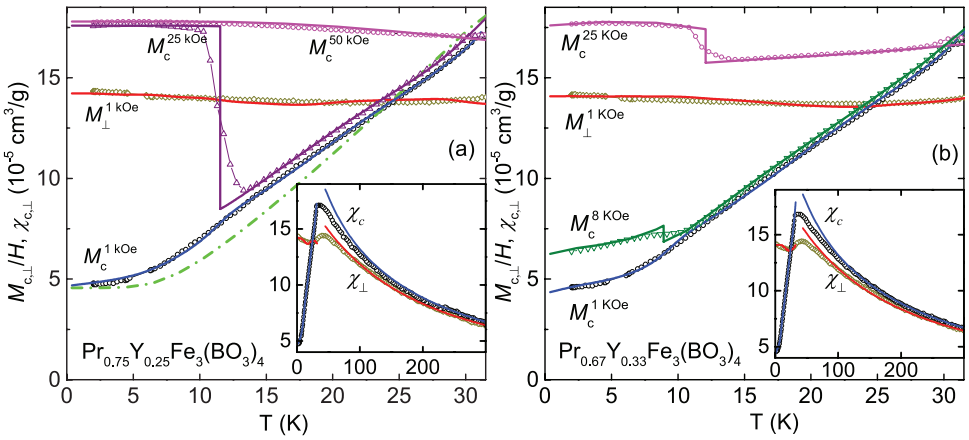

Figure 16. Experimental (symbols) and calculated (lines) temperature dependences of the normalized magnetization $M_{c,\perp}/H$ for $T < T_N$ at the indicated fields and the initial magnetic susceptibility $\chi_{c,\perp}(T)$ at $H_{c,\perp} = 1$ kOe (inset) for $Pr_{0.75}Y_{0.25}Fe_3(BO_3)_4$ (a) and $Pr_{0.67}Y_{0.33}Fe_3(BO_3)_4$ (b).

$$M_a = \frac{1}{2}\left[\frac{1}{3}(M_0^{Fe} - m_{1(0)a}^{Pr_x} + m_{2(0)a}^{Pr_x}) + \frac{2}{3}(M_{60}^{Fe} + m_{1(60)a}^{Pr_x} - m_{2(60)a}^{Pr_x})\right] \quad (9)$$

describes the experimental curve $M_\perp(H)$ well (see figures 13–15). In equation (9) $M_0^{Fe} = M_{1(0)}^{Fe}\sin(\theta_1) - M_{2(0)}^{Fe}\sin(\theta_2)$ is the contribution of iron to the magnetization of the domain $L_{0\perp}$ with consideration for the projection onto the basal plane, and $M_{60}^{Fe} = M_{1(60)}^{Fe}\sin(\theta_1)\cos(\varphi_1) + M_{2(60)}^{Fe}\sin(\theta_2)\cos(\varphi_2)$ is the contribution of iron to the magnetization of the domain L_{60ab} with consideration for the projection onto the basal plane and axis a (see scheme e in figure 10).

In the field H_{SR} a spin-reorientation transition into the flop state with magnetic moments almost perpendicular to the field takes place in the domain L_0, and its magnetization with consideration for the projection onto plane ab is now$M_{flop}^{Fe} = 2M_1^{Fe}\sin(\theta_1)\cos(\varphi_1)$ (see scheme f in figure 10). As a result, the magnetization of the compound at $H > H_{SR}$ is determined by equation (9) upon the substitution of M_0^{Fe} by M_{flop}^{Fe}. When the field $\mathbf{H}\|\mathbf{a}$ increases further, the rotation of $\mathbf{M}_{1,2(60)}^{Fe}$ continues, and starting from fields of about 10 kOe where the domain structure becomes saturated, the resulting magnetization is determined as for the SF state of the entire crystal.

It can be seen from figures 13–15 that the calculated magnetization curves $M_\perp(H)$, which are characterized by the small magnetization jumps, can describe the experimental curves if we take into account the fact that these jumps should be smeared out in a real sample due to the arbitrary orientation of the field in the basal plane, which is different from that shown in figure 10(e). Note that the rotations and jumps of the magnetic moments of the Fe ions in the domains are accompanied by corresponding changes to the orientations of the magnetic moments of the Pr subsystem.

5.3. Temperature dependences of magnetization

Both the iron subsystem ordered at $T < T_N$ and the rare-earth subsystem magnetized by the *f–d* interaction contribute to the initial magnetic susceptibility of $Pr_xY_{1-x}Fe_3(BO_3)_4$. Figures 16 and 17 show the experimental and calculated temperature dependences of the magnetization $M_{c,\perp}(T)$ for $T < T_N$ and the magnetic susceptibility $\chi_{c,\perp}(T)$ for $T = 2$–300 K (in the insets) at $H = 1$ kOe. In the following we explain in detail how the theoretical temperature dependences have been calculated.

As depicted in the insets of figures 16 and 17, the magnetic susceptibility $\chi_c(T)$ measured along the trigonal axis in compounds $Pr_xY_{1-x}Fe_3(BO_3)_4$ is in the paramagnetic region $T > T_N$ slightly higher than the perpendicular susceptibility $\chi_\perp(T)$. This is true for all compounds containing praseodymium, including the non-doped $PrFe_3(BO_3)_4$, and is practically absent in $YFe_3(BO_3)_4$ [15]. This fact leads to the conclusion that the weak anisotropy of the magnetic susceptibility in the paramagnetic state of $Pr_xY_{1-x}Fe_3(BO_3)_4$ is mainly caused by the contribution of the Pr subsystem. Our calculations confirm such a conclusion.

It can be seen from the figures 16 and 17 insets that the agreement between the calculated and experimental susceptibilities for $Pr_xY_{1-x}Fe_3(BO_3)_4$ with $x = 0.75$ and 0.67 is good for $T > 100$ K and $T < T_N$, and less satisfactory on approaching the Neel temperature. In the paramagnetic state, the experimental temperature dependences are well described by the theoretical ones calculated from the Curie–Weiss law at $T > 100$ K (see solid lines in the insets). Below these temperatures, the antiferromagnetic short-range correlations reduce the magnetization and lead to a deviation from the calculated dependences; these deviations increase when approaching T_N. It was observed that a similar effect is exerted by the short-range correlations in other ferroborate crystals. In particular, short-range correlations were observed via the Mössbauer effect in the paramagnetic state of $YFe_3(BO_3)_4$ up to temperatures of 60 K [27].

When magnetizing in the basal plane with $H = 1$ kOe at $T < T_N$, the contributions from all the possible domains to the magnetization $M_\perp(T)$ are taken into account, and the magnetization of $Pr_xY_{1-x}Fe_3(BO_3)_4$ proceeds similarly to the magnetization processes described above when calculating the magnetization M_a (equation (9)).

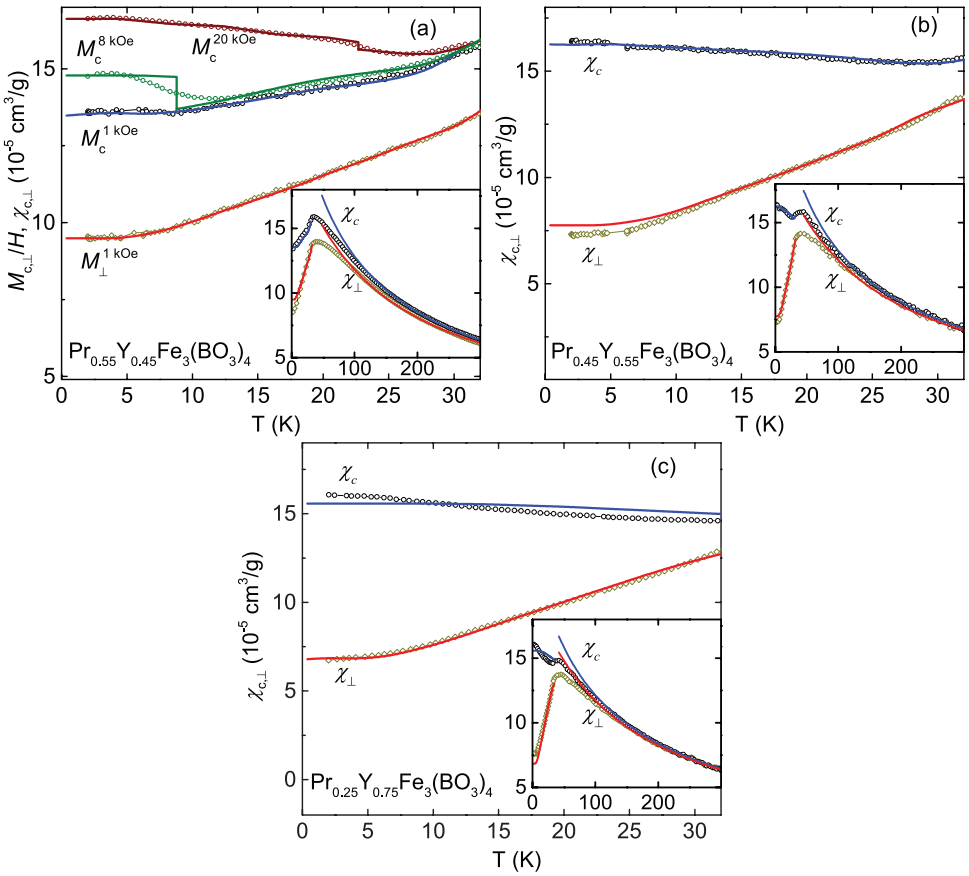

Figure 17. Experimental (symbols) and calculated (lines) temperature dependences of the normalized magnetization $M_{c,\perp}/H$ for $T < T_N$ at the indicated fields and the initial magnetic susceptibility $\chi_{c,\perp}(T)$ at $H_{c,\perp} = 1$ kOe (inset) for $Pr_{0.55}Y_{0.45}Fe_3(BO_3)_4$ (a), $Pr_{0.45}Y_{0.55}Fe_3(BO_3)_4$ (b) and $Pr_{0.25}Y_{0.75}Fe_3(BO_3)_4$ (c).

For the compound with $x = 0.75$, the theoretical curve calculated by assuming that the EA state persists from low temperatures up to T_N is given as a comparison in figure 16 (green dashed line). It is evident that such an assumption only allows a qualitative description of the experimental data. The calculations showed that the apparent discrepancies between the calculated and experimental dependences are associated with the INC phase and a nonmonotonic change in the inclination angle $\theta^{Fe}(T)$ with temperature. In the case of $H = 0$, the nonmonotonic dependences of $\theta^{Fe}_{exp}(T)$ were determined via neutron diffraction for compounds with $x = 0.67$, 0.55, 0.45 [18]. The influence of an applied field **H**||**c** or **H** $\perp$ **c** on $\theta^{Fe}_{exp}(T)$ is, however, not known. Therefore, the temperature dependences of the anisotropy constants $K_2^{Fe}(T)$ and $K_4^{Fe}(T)$ that were found in [18] to reproduce the main features of the experimental dependences of $\theta^{Fe}_{exp}(T)$ at $H = 0$ were used at the initial stage for the description of the experimental temperature dependences of the magnetizations $M_{c,\perp}(T)$. The calculated dependences obtained at this stage did not reflect all the peculiarities of the experimental dependences $M_{c,\perp}(T)$, e.g. a slightly pronounced maximum near 12 K in the experimental curves $M_c^{1\ kOe}(T)$ for compounds with $x = 0.75$ and 0.67 (see figures 16(a) and (b)). Small corrections of $K_2^{Fe}(T)$ and K_4^{Fe}(T) were performed to achieve the best description of the experimental data; the calculated dependences of the magnetizations are shown in figures 16 and 17 (solid lines). The calculations show that the nonmonotonic behavior of the temperature dependences of the inclination angle should be taken into account for the correct description of the temperature dependences of the magnetizations $M_{c,\perp}(T)$ for all the compounds $Pr_xY_{1-x}Fe_3(BO_3)_4$ with an INC magnetic structure.

Note that the slightly pronounced maxima near 12 K in the experimental curves $M_c^{1\ kOe}(T)$ for $x = 0.75$, 0.67, which are explained by the nonmonotonicity of the temperature dependences of the inclination angle $\theta^{Fe}_{exp}(T)$, cannot be related to a Schottky anomaly because the splitting between the lowest energy levels $\Delta \approx 72\ cm^{-1}$ at $T \approx 12$ K is too large.

Figures 16 and 17 also show the theoretical description of the curves $M_c(T)$ in magnetic fields larger than 1 kOe. The nature of the observed jumps in the magnetization becomes clear when these temperature dependences are compared with the field dependences measured at different fixed temperatures. For example, figure 11 shows the field dependence of the quenched $Pr_{0.75}Y_{0.25}Fe_3(BO_3)_4$ with the magnetization jump corresponding to the transition between the INC and the SF states. The inset in figure 11(c) shows the temperature dependence of the critical field for this sample representing the phase boundary between the states at the coordinates 'field–temperature'. The jump of the magnetization found in the field of 25 kOe near $T = 12$ K for the

quenched sample (see figure 16(a)) is just the transition between the SF (scheme d in figure 10) and INC (scheme c) states occurring with changing temperature. In the phase diagram, this transition corresponds to the crossing of the boundary between the states along the dotted line shown in the inset of figure 11(c). In this case the temperature dependence $M_c(T)$ was calculated using equation (8) in the SF state below 12 K and equation (7) in the INC state above this temperature.

The comparable but smoother anomalies present in the curves $M_c(T)$ for compositions with $x = 0.67$ and 0.55 were described theoretically in a similar way (see figures 16(b) and 17(a)).

6. Conclusions

Single crystals of the $Pr_xY_{1-x}Fe_3(BO_3)_4$ family of about 4–6 mm in size were grown from the flux. The temperature and field dependences of the magnetization were studied for all the compounds with $x = 0.25 \div 1$. Magnetic resonance studies were used to identify some of the magnetic states.

A gradual transition from the EA structure characteristic of pure $PrFe_3(BO_3)$ to the EP structure formed in $YFe_3(BO_3)_4$ occurs with the diamagnetic dilution of the rare-earth subsystem. This transformation is determined by the decreasing contribution of the praseodymium subsystem to the total magnetic anisotropy of the crystal that occurs upon dilution. The transformation occurs through an INC magnetic structure, which is established at intermediate values of the diamagnetic substitution. The concentration dependences of the Neel temperature and the inclination angle of the antiferromagnetic vector of the iron subsystem relative to the basal plane measured at $T = 3$ K are presented.

A theoretical approach based on a crystal-field model for the Pr^{3+} ion and the molecular-field approximation allowed us to describe the magnetic characteristics of $Pr_xY_{1-x}Fe_3(BO_3)_4$ with good agreement between the experimental and calculated temperature and field dependences of the magnetization curves $M_{c,\perp}(H)$ and $M_{c,\perp}(T)$. A detailed comparison with the experimental data allowed us to determine parameters that characterize the exchange interaction, the magnetic anisotropy of the iron subsystem and the crystal field parameters of the Pr ion for every compound in the $Pr_xY_{1-x}Fe_3(BO_3)_4$ family. The important role of the anisotropy constant K_4^{Fe} in stabilizing the INC state was established.

A reorientation into an SF phase occurs on the application of a magnetic field along the trigonal axis of a crystal with an EA structure where the antiferromagnetic vector in the zero field is oriented along the trigonal axis or one that is in an INC state with the inclination angle not too large ($x = 0.55 \div 1.0$). The transition between these states can take place when either the temperature or the magnetic field $\mathbf{H}\|\mathbf{c}$ changes. The magnetic phase diagram in the H–T coordinates is constructed for one of the compounds.

A two-step jump of $M_c(H)$ appears in the compounds with $x = 0.75$ and 0.67 that were prepared by slow cooling. Such a two-step reorientation process into the SF state is explained by the emergence of an interjacent INC state that is stable in a small range of magnetic field values. This interjacent INC state is characterized by the magnetic moments of the iron subsystem with a definite inclination angle to the basal plane that is smaller than that in the initial zero-field INC state. An inhomogeneous strain arising in the quenched samples of the same composition prevents the formation of the interjacent state, and the spin reorientation occurs directly into the flop state either throughout the crystal or in the greater part of it, which is the most strained. The magnetic moments of the Fe and Pr ions in compounds with $x < 0.45$ lie in the basal plane or close to it. Some features associated with the dynamics of the 120° domain structure are observed in low fields while magnetizing in the basal plane. All of these features are well described in the framework of the proposed theoretical approach.

Acknowledgment

This work was supported by the Russian Foundation for Basic Research (project no. 15-42-04186_r_sibir'_a).

References

[1] Zvezdin A K, Vorob'ev G P, Kadomtseva A M, Popov Yu F, Pyatakov A P, Bezmaternykh L N, Kuvardin A V and Popova E A 2006 *JETP Lett.* **83** 509
[2] Popova E A *et al* 2007 *Phys. Rev.* B **75** 224413
[3] Chaudhury R P, Yen F, Lorenz B, Sun Y Y, Bezmaternykh L N, Temerov V L and Chu C W 2009 *Phys. Rev.* B **80** 104424
[4] Kadomtseva A M *et al* 2010 *Low Temp. Phys.* **36** 511
[5] Usui T *et al* 2014 *Nat. Mater.* **13** 611
[6] Hinatsu Y, Doi Y, Ito K, Wakeshima M and Alemi A 2003 *J. Solid State Chem.* **172** 438
[7] Klimin S A, Fausti D, Meetsma A, Bezmaternykh L N, van Loosdrecht P H M and Palstra T T M 2005 *Acta Crystallogr.* B **61** 481
[8] Ritter C, Vorotynov A, Pankrats A, Petrakovskii G, Temerov V, Gudim I and Szymczak R 2008 *J. Phys.: Condens. Matter* **20** 365209
[9] Ritter C, Balaev A, Vorotynov A, Petrakovski G, Velikanov D, Temerov V and Gudim I 2007 *J. Phys.: Condens. Matter* **19** 196227
[10] Ritter C, Vorotynov A, Pankrats A, Petrakovski G, Temerov V, Gudim I and Szymczak R 2010 *J. Phys.: Condens. Matter* **22** 206002
[11] Janoschek M, Fischer P, Schefer J, Roessli B, Pomjakushin V, Meven M, Petricek V, Petrakovskii G and Bezmaternykh L 2010 *Phys. Rev.* B **81** 094429
[12] Mo H, Nelson C S, Bezmaternykh L N and Temerov V T 2008 *Phys. Rev.* B **78** 214407
[13] Demidov A A, Gudim I A and Eremin E V 2012 *JETP* **114** 259
[14] Pankrats A I, Petrakovskii G A, Tugarinov V I, Kartashev A V and Temerov V L 2011 *JETP* **113** 483
[15] Popova E A, Vasiliev A N, Temerov V L, Bezmaternykh L N, Tristan N, Klingeler R and Buchner B 2010 *J. Phys.: Condens. Matter* **22** 116006
[16] Pankrats A, Petrakovskii G, Bezmaternykh L and Temerov V 2008 *Phys. Solid State* **50** 79
[17] Kadomtseva A M, Popov Yu F, Vorb'ev G P, Mukhin A A, Ivanov V Yu, Kuz'menko A M and Bezmaternykh L N 2008 *JETP Lett.* **87** 39

[18] Ritter C, Pankrats A I, Demidov A A, Velikanov D A, Temerov V L and Gudim I A 2015 *Phys. Rev.* B **91** 134416
[19] Bezmaternykh L N, Temerov V L, Gudim I A and Stolbovaya N A 2005 *Crystallogr. Rep.* **50** 97
[20] Volkov D V, Demidov A A and Kolmakova N P 2007 *JETP* **104** 897
[21] Gurevich A G 1973 *Magnetic Resonance in Ferrites and Antiferromagnets* (Moscow: Nauka) p 591
[22] Demidov A A 2014 *Physica* B **440** 73
[23] Demidov A A, Kolmakova N P, Volkov D V and Vasiliev A N 2009 *Physica* B **404** 213
[24] Popova M N, Stanislavchuk T N, Malkin B Z and Bezmaternykh L N 2009 *Phys. Rev.* B **80** 195101
[25] Popova M N, Stanislavchuk T N, Malkin B Z and Bezmaternykh L N 2009 *Phys. Rev. Lett.* **102** 187403
[26] Boldyrev K N, Stanislavchuk T N, Sirenko A A, Bezmaternykh L N and Popova M N 2014 *Phys. Rev.* B **90** 121101
[27] Rebbouh L, Desautels R D, Ritter C, Cadogan J M, Temerov V, Pankrats A and van Lierop J 2011 *Phys. Rev.* B **83** 140406